https://doi.org/10.5194/egusphere-2024-166
Preprint. Discussion started: 27 February 2024

Earthquakes triggered by the subsurface undrained response to reservoir-impoundment at Irapé, Brazil

Haris Raza[1,2,3]*, George Sand França[1,2], Eveline Sayão[1], Victor Vilarrasa[3]

[1]Seismological Observatory, Graduate Program in Geology, Institute of Geosciences, University of Brasília, Campus Darcy Ribeiro, 70297-400 Brasília, Brazil

[2]Institute of Astronomy, Geophysics and Atmospheric Sciences, University of São Paulo, 05508-090, São Paulo, Brazil

[3]Global Change Research Group (GCRG), IMEDEA, CSIC-UIB, 07190 Esporles, Spain

*Correspondence to: Haris Raza (harisraza90@yahoo.com), Victor Vilarrasa (victor.vilarrasa@csic.es)

Abstract

The necessity to reduce carbon emissions to mitigate climate change is accelerating the transition from fossil fuels to renewable energy sources. Specifically, hydropower, in particular, has emerged as a prominent and safe renewable energy source, but entails reservoir-triggered seismicity (RTS). This phenomenon causes significant challenges for safe reservoir management. Irapé, in Brazil, is a prominent RTS site where seismicity surged after reservoir filling, with a maximum event of magnitude 3.0 in May 2006, just six months after the start of reservoir impoundment. Despite more than a decade has passed since the seismicity occurred, the factors governing these earthquakes and their connection to subsurface rock properties remain poorly understood. Here, we attempt to understand the potential causes of RTS at Irapé dam, which is the highest dam in Brazil with 208 m, and the second highest in South America. Permeability and porosity measurements of cylindrical cores from hard and intact rock samples, which have been extracted near the RTS zone, by pitting 10 cm from the surface, reveal a low-permeability rock. Porosity values range from 6.340 to 14.734%. Only 3 out of the 11 tested samples present permeability higher than the lowest measurable value of the apparatus (0.002 mD), with the highest permeability being 0.0098 mD. The undrained response of the low-permeability rock placed below the reservoir results in an instantaneous increase in pore pressure and poroelastic stress changes due to elastic compression, which brings potential faults located below the reservoir closer to failure conditions. According to our analytical calculations, the increase in 136 m of the reservoir-water level caused a 0.54 MPa pore pressure buildup at the depth of the Magnitude 3.0 earthquake, i.e., 3.88 km, resulting in an increase of 0.82 MPa in the vertical effective stress and a decrease of 0.34 MPa in the

https://doi.org/10.5194/egusphere-2024-166
Preprint. Discussion started: 27 February 2024

horizontal effective stress. These changes resulted in an increase in the deviatoric stress that led to fault destabilization, causing the RTS. The laboratory measurements and analytical calculations corroborate the hypothesis that the initial seismic activity was induced by the undrained subsurface response to the reservoir loading at Irapé.

Keywords: Brazil, Reservoir-triggered seismicity, Permeability, Porosity, Fault, Reservoir-management

1.Introduction

Reservoir impoundment, deep underground mining, and fluid injection into and withdrawal from the subsurface are some of the well-known causes of induced/triggered seismicity which have become a global issue in the past few decades (McGarr et al., 2002; Foulger et al., 2018; Kivi et al., 2023). The understanding and identification of these types of human-induced earthquakes is crucial in terms of environmental and economic impact, as well as for socio-political and scientific discussion (Gonzalez et al., 2012; Vilarrasa et al., 2019). Recently, the debate over potential induced or triggered nature of cases of felt seismicity has intensified, such as the Oklahoma earthquakes of Mw 5.7 in 2011 and of Mw 5.8 in 2016 (Ellsworth, 2013; Keranen et al., 2013; Yeck et al., 2017), Emilia, Italy, earthquakes of Mw 6.1 and 5.9 in 2012 (Cesca et al., 2013a), Pohang, South Korea, earthquake of Mw 5.5 in 2017 (Grigoli et al., 2018; Kim et al., 2018), Lorca, Spain, earthquake of Mw 5.1 in 2011 (González et al., 2012), and Castor, Spain, earthquake sequence of Mw 4.1 in 2013 (Cesca et al., 2014; Vilarrasa et al., 2021; Vilarrasa et al., 2022), to name a few. Apart from the possibility of injuring people and damaging infrastructure, such earthquakes can have a negative public perception leading to project cancellation (Boyet et al., 2023a).

The first reservoir-triggered seismicity (RTS) case was observed during the filling of Lake Mead at the Hoover Reservoir (US) in the mid-1930s, with ~M4.0 (Carder 1945). Major worldwide RTS cases were detected in the 1960s, such as the M6.1 Hsinenghiang (China) in 1962, Kariba (Zambia) M6.2 in 1963, Kremasta (Greece) M6.3 in 1966, and Koyna (India) M6.3 in 1967 (Gupta, 2002). To date, over 150 RTS cases have been documented (Wilson et al., 2017; Foulger et al., 2018). Studies to understand

https://doi.org/10.5194/egusphere-2024-166
Preprint. Discussion started: 27 February 2024

the triggering mechanisms of RTS show that pore pressure changes in the order of a few tenth of MPa and the associated poroelastic stress changes are sufficient to reactivate deep faults (Rice and Cleary, 1976; Simpson, 1976; Bell and Nur, 1978; Talwani and Acree, 1985; Roeloffs, 1988; Simpson et al., 1988).

RTS is generally controlled by the stress state, the geological and hydrogeological properties of the region, and the water-level changes at the reservoir. The perturbation caused by the changes in water-level results in the loading and/or unloading of the subsurface, which may respond in an undrained or drained way. An undrained response leads to an instantaneous pore pressure buildup that is proportional to the height of the reservoir load. In contrast, a drained response leads to pore pressure diffusion into the rock that causes progressive pore pressure build-up as the pressure front propagates into the rock (Table 1). In general, RTS magnitudes are smaller for undrained responses than drained ones (Simpson et al.,1988). The interactions and comprehensive analysis of these two responses are key to improving the forecasting and mitigation of RTS hazard.

Table 1. The time-distribution types of responses to reservoir-triggered earthquakes (by Simpson, 1988)

Response type	Mechanism	Description	Main features	Cases
Instantaneous response	Instantaneous elastic response and undrained response due to reservoir loading	This type of RTS increases immediately after the initial impoundment of reservoir or changes rapidly after rapid changes in the water level.	Changes in water level have a strong correlation with the change of seismicity, this generally occurs around the reservoir area, and the earthquake magnitude is small, the majority of them are swarm seismicity.	Monticello, Manico-3, Nurek, Kariba, Kremesta *Irapé (this paper)*
Delayed response	Increase of pore pressure caused by pressure diffusion through permeable rock below the reservoir	It is only after a period of reservoir impoundment that the seismicity changes continuously	No significant correlation between changes in water level and seismicity, the time delay is obvious, the magnitude is generally large, and the earthquake occurrence point is not limited.	Koyna, Aswan, Oroville

The RTS cases are booming around the world, with Brazil being one of the concerned countries with 29 RTS cases to date (Sayão et al., 2020). The study of RTS in Brazil started in 1972 with the M3.7 at

https://doi.org/10.5194/egusphere-2024-166
Preprint. Discussion started: 27 February 2024

Carmo do Cajuru reservoir, southeast Brazil (Foulger et al., 2018). The largest recorded event, a M4.2 in 1974, caused damage to several buildings without any fatalities and was associated with nearby reservoirs at Porto Colombia and Volta Grande, both of which started damming in the early 1970s (Sayão et al., 2020).

The Irapé dam, located in the state of Minas Gerais, Brazil, is the highest dam in Brazil with about 208 m, and the second highest in South America (França et al., 2010). The Irapé hydropower plant lies in the vicinity of Jequitinhonha River. Seismicity started to increase immediately after the impoundment of the reservoir and completion of the dam with the maximum event of M3.0 occurred on 14 May 2006, coinciding with the peak water level of the dam. The significant magnitude of the earthquake and the early occurrence after-filling of the reservoir impoundment has raised questions about the triggering mechanisms of this RTS. Understanding these mechanisms is crucial for ensuring the safety of infrastructure around the Irapé reservoir and for the local population.

In this study, we aim to investigate the potential causes of the main RTS event at Irapé. We initially elaborate on the geological setting and rock characteristics in the vicinity of the reservoir. We explain the characteristics of the RTS at Irapé, including the temporal evolution of the seismicity, which occurred in the short period from December 2005 to May 2006 and the location of the main event based on the local velocity model. Then, we present the performed permeability and porosity tests of cylindrical cores from hard and intact rock samples, which have been extracted near the RTS zone to identify and describe the primary role of porosity and permeability. We perform analytical calculations to estimate that pore pressure and poroelastic stresses in response to the highest water level of the reservoir filling and the time that would take for the pore pressure diffusion front to reach the depth of the main event. We present evidence that the cause of RTS at Irapé was the undrained response of the subsurface to reservoir impoundment.

2. Geological setting and RTS at Irapé

2.1 Geological setting

https://doi.org/10.5194/egusphere-2024-166
Preprint. Discussion started: 27 February 2024

The area of Irapé is located within the domain of the Pre-Folding Belt Cambrian Araçuaí, which is oriented approximately in a north-south direction and defines the eastern part of the São Francisco Craton in the State of Minas Gerais (Almeida, 1977). Approximately 80% of the reservoir area in Irapé corresponds to the Chapada Acauã Formation. The Chapada Acauã Formation, which has been investigated near the Irapé Shear Zone (Araujo et al., 2010), consists of carbonaceous mica-schist rocks, locally with pyrite, garnet, or graphite (Lima, 2002). This rock is intensely deformed, with the formation and rotation of quartz sub-grains and migration of grain edges. It represents, together with the Nova Aurora Formation, typical sedimentation of passive margin associated with deposition in the Macaúbas Basin. To the east of the Chapada Acauã Formation, it is found the Ribeirão da Folha Formation, consisting of mica shales, metaritmitos, quartzite and calc-silicates rock (Figure 1).

https://doi.org/10.5194/egusphere-2024-166
Preprint. Discussion started: 27 February 2024

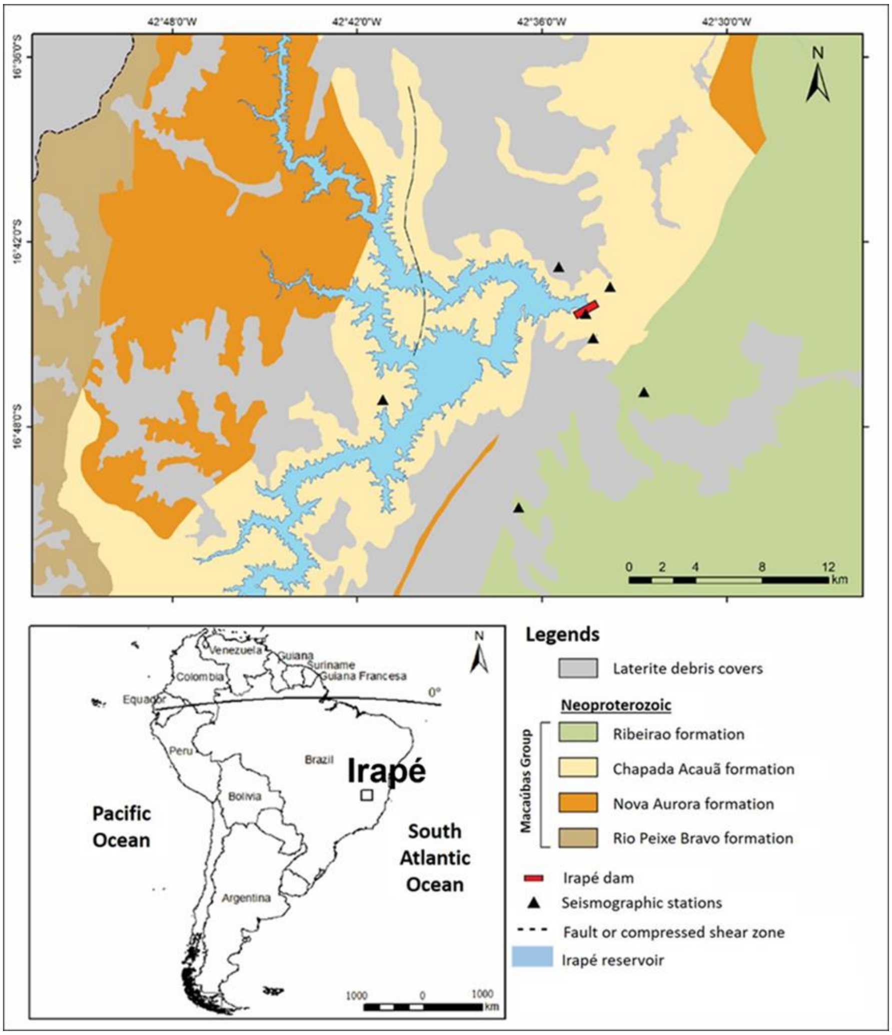

Figure 1. Geological map of Irapé reservoir and surrounding area

2.2 Background on the reservoir-triggered seismicity at Irapé

The Irapé reservoir covers an area of 137.8 km^2 with a reservoir volume of 5.964 km^3. The dam was constructed on the Jequitinhonha River, filling the reservoir to a maximum height of 137 meters (Figure 1 and Table 2). The dam area was monitored by a three-component seismic network at three stations prior to 3 years of its impoundment, which started on 7 December 2005. These stations did not detect any seismicity before the impoundment (Chimpliganond et al., 2007).

https://doi.org/10.5194/egusphere-2024-166
Preprint. Discussion started: 27 February 2024

Table 2. Characteristics of the main RTS event at Irapé (França et al., 2010)

Dam height (m)	Length (m)	Volume (km^3)	Max. reservoir water depth (m)	Reservoir area (km^2)	Seismicity type	Date	Magnitude (mR)	Io (MMI)	ΔT(yr)
208	540	5.964	137	137.8	Initial	14 May 2006	3.0	III-IV	0.5

ΔT: interval time (years) since the start of filling/impoundment; MMI: modified Mercalli Intensity scale, mR: magnitude Regional.

Microearthquakes started to be detected just one day after the impoundment began, exceeding 300 microearthquakes by October 2006. The largest event occurred on 14 May 2006 with a M3.0 that was felt at the reservoir area (Chimpliganond et al., 2007; França et al., 2010). The seismicity occurred within a small area, with epicentres in the lake and its nearby margins (less than 3 km from the narrow lake), close to the dam axis. The evident time correlation between the start of the impoundment of the lake and the occurrence of seismicity suggests a causative relationship for this seismicity (Figures 2 and 3). The spatial distribution of the epicentres also suggests the hypothesis that this is another case of RTS of the initial response type.

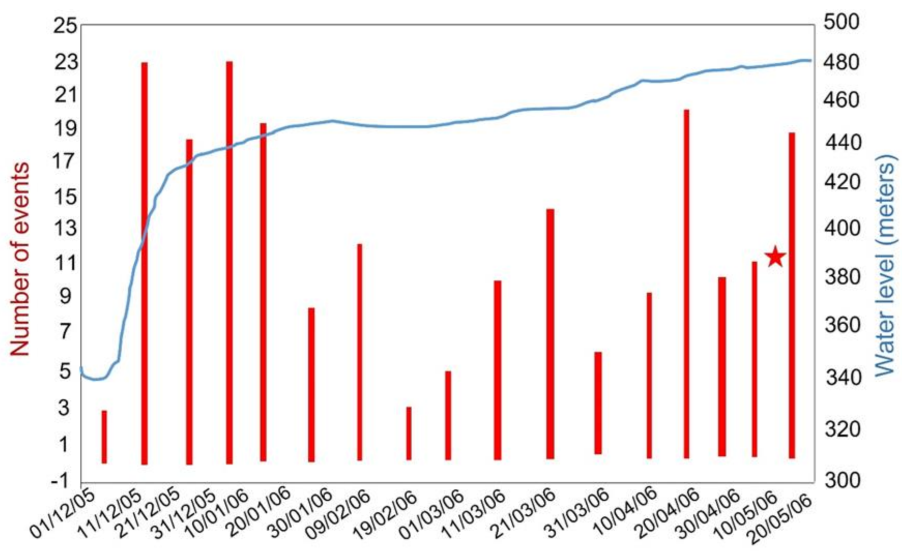

Figure 2. Temporal evolution of RTS at Irapé by ten days. Number of events during December 2005 to May 2006 (histogram) at Irapé and average water elevation above the mean sea level (blue line) are

https://doi.org/10.5194/egusphere-2024-166
Preprint. Discussion started: 27 February 2024

illustrated. The red star indicates the time when the main and largest event occurred, M3.0 on 14 May 2006 (modified from Silva et al., 2014).

The events were analysed using the program Seismic Analysis Code (Goldstein and Snoke,2005), in which the arrival of the P and S waves and the polarity are considered. The hypocentre location of the events that were recorded by three stations was computed with the program HYPO71 (Lee and Lahr, 1975). The analysis of seismograms went through a double-checks routine (Silva et al., 2014).

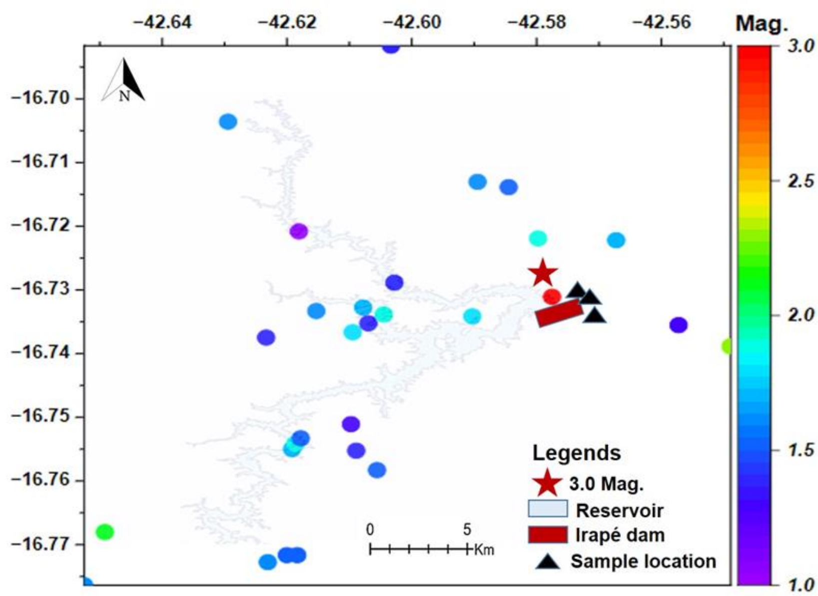

Figure 3. RTS Distribution in the initial period with location and magnitude (see colour scale), the red star is the main event felt near the dam and black triangles denote the samples location.

Velocity models were adopted based on a deep seismic refraction survey in combination with local geological interpretations and studies of the crustal structure in south-eastern Brazil to locate seismic events in the Irapé area (Assumpção et al., 2012). The local velocity model consists of a superficial 4.8 km-thick layer with a P-wave velocity (V_p) of 4.5 km/s, representing the mica-schist to graphite-schist rocks from surface, and a second layer from schist to crystalline basement rocks with a thickness of 11.2 km with P-wave velocity (V_p) of 6 km/s (Marshak et al., 2006; Silva et al., 2014).

https://doi.org/10.5194/egusphere-2024-166
Preprint. Discussion started: 27 February 2024

The repetition of a structural trend in the NE-SW direction originates from the geological and geophysical structuring of the crust (Silva et al., 2014). The stress regime in the Irapé region has been estimated to be a normal faulting stress regime. The accuracy of the focal mechanisms remains a subject of debate due to the low quality of the seismic data recorded by analogue seismograms and uncertainties associated with the velocity model. Consequently, the focal mechanisms of the May 14, 2006, M3.0 earthquake have not been resolved yet (Silva et al., 2014).

3.Materials and methodology

We inspected the Irapé site and surrounding areas as well as the outcrops. The dam area is surrounded by mica-schist rock, which is shiny, ranging from blackish to medium grey in colour, with foliated, fine to medium-grained textures. According to the local velocity model, there is a superficial layer that is 4.8-km thick, representing mica-schist to graphite-schist rocks at the surface. Below that, there is a second layer that is 11.2-km thick, consisting of crystalline basement rock. Measurements from these samples are crucial for understanding the estimated permeability beneath the subsurface in the context of the main event, which occurred at a depth of 3.88 km (França et al., 2010). Since the epicenter of the main event was located about 1 km away from the dam, we collected bulk rock samples from different locations around the dam, as well as nearby outcrops, by digging pits that were 0.10-m deep.

3.1 Laboratory experiments

We have extracted cylindrical core samples perpendicular to the bedding planes of mica-schist rock. We have performed tests on three sets of samples, with a total of 11 core samples, of hard and intact samples because the rest of the samples were fragile and fractured during the coring from bulk samples (Table 3). The retrieved cylindrical plugs have a length ranging from 3.8 to 5.0 cm and a diameter of 2.50 cm, which meets the International standard criteria (Core Lab) to measure core plug samples by Ultra-Pore 300 and Ultra-Perm 610 (Figures 4).

https://doi.org/10.5194/egusphere-2024-166
Preprint. Discussion started: 27 February 2024

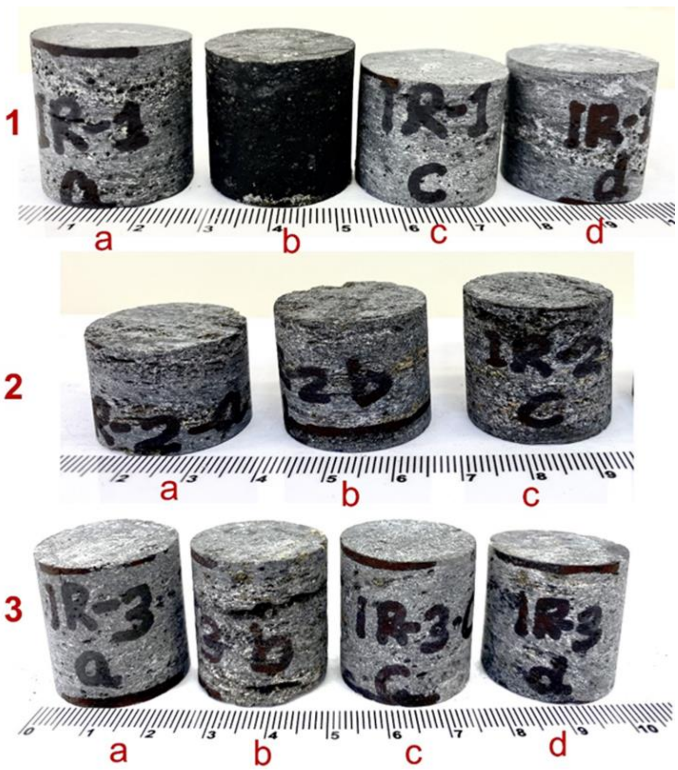

Figure 4. The three sets of mica-schist rock samples (1, 2, and 3) after cylindrical coring from bulk samples (⊥ coring of cylindrical plugs has been done by loading perpendicular to the bedding planes).

We conduct porosity measurements using the Ultra-Pore 300, which is manufactured by Core Lab Instruments in Texas, USA. The Ultra-Pore 300 is a gas expansion helium pycnometer specifically designed for determining the grain volume or pore volume of both core plug and full-diameter samples. To achieve this, we utilized matrix cups designed for samples with diameters ranging from 2.5 to 3.8 cm, equipped with a Setra 204 transducer rated for pressures ranging from 0 to 1.72 MPa. We determined the pore volume using the nitrogen gas (N_2) expansion technique (API,1998; Ceia et al., 2019).

We measure the intrinsic permeability of rock samples using Ultra-Perm 610 Permeameter. This precision equipment, which controls backpressure, maintains a constant rate or mean pressure at 0.69 MPa. Before testing, samples are cleaned with soxhlet equipment and toluene, followed by drying in an

https://doi.org/10.5194/egusphere-2024-166
Preprint. Discussion started: 27 February 2024

oven. The permeability measurements included a permeameter, nitrogen source, stopwatch, a core holder, a bubble tube, and a digital calliper. The core holder is pressurized to 3.45 MPa confining pressure using compressed air. The bubbles passing through a burette are timed, and outflow gas volume is recorded. The permeability is calculated using Darcy's law, considering core dimensions. Hard rock core samples, like mica-schist, require long stabilization times due to the low permeability.

3.2 Analytical calculations of undrained pore pressure and stress changes

Reservoir impoundment causes an undrained effect in the subsurface that manifests as an instantaneous pore pressure and stress changes below the reservoir (Skempton, 1954). The change in the vertical stress, $\Delta\sigma_v$, equals the weight of the water level rise. The horizontal stress, assuming iodometric conditions, changes proportionally to pore pressure changes as (Rutqvist, 2012)

$$\Delta\sigma_h = \alpha \frac{(1-2\nu)}{(1-\nu)} \Delta p \,, \quad (1)$$

where $\Delta\sigma_h$ is the horizontal stress change, α is Biot's coefficient, ν is Poisson's ratio and Δp is the pore pressure change. Additionally, in an isotropic and homogeneous poroelastic material subject to undrained conditions, the change in pore pressure resulting from a change in stress can be computed as (e.g., Rice and Cleary, 1976; Cocco and Rice, 2002)

$$\Delta p = \frac{-B}{3} \Delta\sigma_{kk} \,, \quad (2)$$

where $\Delta\sigma_{kk} = \Delta\sigma_v + 2\Delta\sigma_h$, $\Delta\sigma_{kk}$ is the stress change and B is the Skempton's coefficient of mica-schist rock (Roeloffs, 1988). Equations (1) and (2) constitute a system of two equations with two unknowns. Its resolution yields the undrained pore pressure change as

$$\Delta p = \frac{B}{3} \frac{\Delta\sigma_v}{\left(1 - \frac{2B\alpha}{3}\frac{(1-2\nu)}{(1-\nu)}\right)}. \quad (3)$$

3.3 Analytical calculations of the time at which the pore pressure diffusion front reaches the depth of the earthquake

The advancement of the pore pressure front within the subsurface is controlled by diffusivity

https://doi.org/10.5194/egusphere-2024-166
Preprint. Discussion started: 27 February 2024

$$D = \frac{k\rho g}{\mu S_s} \tag{4}$$

where, D is diffusivity, k is the intrinsic permeability, ρ is water density, g is gravity, μ is water viscosity, and S_s is the specific storage coefficient. The time at which the pore pressure front reaches a certain distance r is given by

$$t = \frac{r^2}{D} \tag{5}$$

4.Results

4.1 Porosity and permeability measurements

The results of our laboratory measurements are provided in Table 3. These data are subject to measurement uncertainties inherent to the experimental equipment used according to the standard procedure. Laboratory measurements of samples of mica-schist reveal a low permeability (Table 3 and Figure 6). The maximum permeability is 0.0098 mD, but most of the samples present a permeability below the precision of the apparatus, i.e., lower than 0.002 mD. Such permeability is in the range of low-permeability rock, which act as a barrier to flow. Most of the samples have a porosity between 6 to 10%, except for two with higher porosity. The low permeability of mica-schist could be explained by the fact that the larger pores are not well connected (Figure 5). In general, there is no correlation between permeability and porosity (Figure 6).

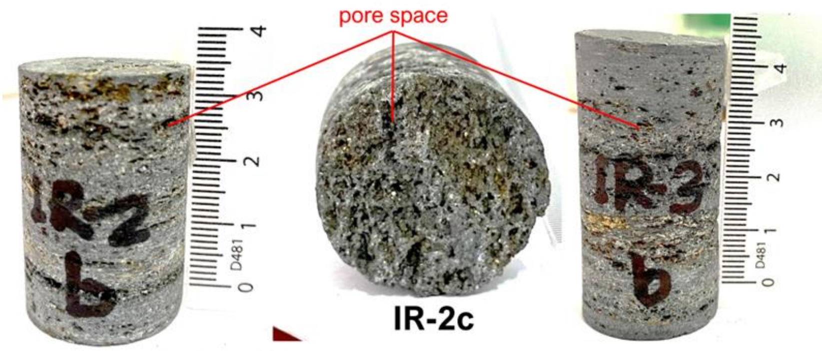

https://doi.org/10.5194/egusphere-2024-166
Preprint. Discussion started: 27 February 2024

Figure 5. Megascopic representation of samples IR-2 b, c, and IR-3b showing pores that are not well-connected.

Table 3. Location of samples with permeability and porosity data from measured cores

Location (lat., long.)	Sample Numbers	Permeability (mD)	Porosity (%)
16.73872, 42.57680	IR-1a	0.002	7.529
	IR-1b	0.002	6.785
	IR-1c	0.002	8.781
	IR-1d	0.0098	6.555
16.74038, 42.57652	IR-2a	0.002	9.490
	IR-2b	0.0038	10.465
	IR-2c	0.0038	14.734
16.72438, 42.56316	IR-3a	0.002	6.943
	IR-3b	0.002	13.323
	IR-3c	0.002	7.126
	IR-3d	0.002	6.340

Experiments loaded perpendicular to bedding plane (⊥)

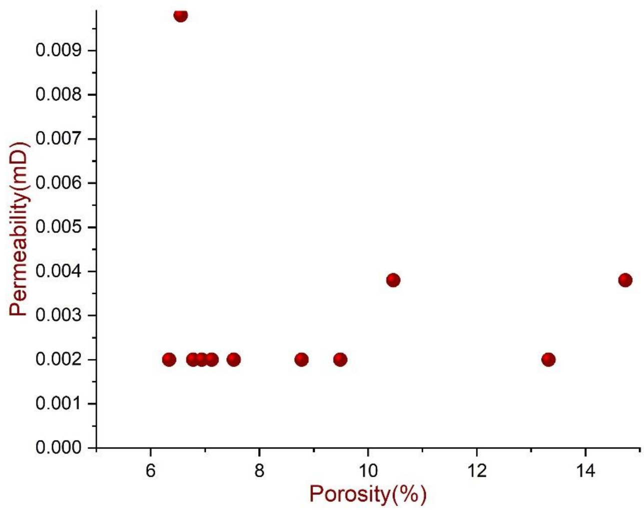

Figure 6. Porosity-permeability relation of mica-schist rock samples.

4.2 Undrained response of rock: changes in pore pressure and stress

The 136 m of water level increase at the time of the M3.0 earthquake resulted in an increase in the vertical stress of 1.36 MPa. To compute the pore pressure change caused by the reservoir impoundment, the Biot coefficient, Skempton's B coefficient and Poisson's ratio of mica-schist are needed (Eq. (3)). Since such measurements are not available, we adopt the values of Opalinus Clay because it is a similar

https://doi.org/10.5194/egusphere-2024-166
Preprint. Discussion started: 27 February 2024

rock to mica-schist. Thus, we assume Skempton's B coefficient of 0.92, undrained Poisson's ratio of 0.39 and Biot's coefficient of 1. With these values, the resulting pore pressure change is 0.54 MPa. Consequently, the horizontal stress change is of 0.19 MPa (Eq. (1)). These pore pressure and stress changes result in a vertical effective stress increase of 0.82 MPa and a horizontal effective stress decrease of 0.34 MPa, increasing the deviatoric stress in more than 1 MPa.

4.3 Pressure diffusion along mica-schist

The measured intrinsic permeability of mica-schist is in the order of 10^{-18} m^2 (Table 3). Assuming a specific storage coefficient in the order of 1.05×10^{-6} m^{-1}, diffusivity (Eq. (4)) results in 9.5×10^{-6} m^2/s. Taking into account that the depth of the M3.0 earthquake occurred at 3.8 km, the time at which the pore pressure front would reach this depth by diffusion (Eq. (5)) is in the order of 50,000 years.

5.Discussion

RTS has been the focus of many studies, but the origin and development of RTS are still unclear in many cases (Gupta et al., 2016; Arora et al., 2018). There is a general consensus that there are two main triggering mechanisms (Simpson et al., 1988). On the one hand, low-permeability rock has an undrained response to the water-level changes of the reservoir, which acts as a loading, instantaneously increasing pore pressure and causing poroelastic stress changes deep underground (Chen and Talwani, 2001; Vilarrasa et al., 2022; Raza et al., 2023). On the other hand, in the presence of permeable rock or a permeable fracture network, pore pressure diffuses downwards, which may eventually trigger an earthquake if a critically stressed fault becomes pressurized (Talwani and Acree, 1985).

At Irapé, the low-permeability of the rock below the reservoir, i.e., mica-schist with permeability in the order of 10^{-18} m^2 or lower, hinders pore pressure diffusion. Given that the hypocentre was located at 3.88 km depth, the pressure propagation front would take in the order of 50,000 years to start pressurizing the depth at which the earthquake was nucleated. Even assuming that the presence of fractures enhanced the rock permeability by three orders of magnitude, which would be the upper limit of observed permeability enhancement of low-permeability rock at the field scale (Neuzil, 1986), the pressure front would take 50 years to reach 3.88 km depth. The necessary permeability of the rock to

https://doi.org/10.5194/egusphere-2024-166
Preprint. Discussion started: 27 February 2024

reach the depth of the largest earthquake within 0.5 years, i.e., the delay of the earthquake with respect to the start of impoundment, would be of 10^{-13} m^2, five orders of magnitude higher than the actual permeability of mica-schist. Such high permeability enhancement is deemed unlikely.

Considering the load caused by the water-level rise in the reservoir of 136 m, the low-permeability mica-schist experienced an undrained response, with subsequent poroelastic stress and pore water changes. We have estimated these changes analytically, finding a vertical effective stress increase of 0.82 MPa, a horizontal effective stress decrease of 0.34 MPa, and a pore pressure increase of 0.54 MPa. Given the normal faulting stress regime at Irapé, these changes cause an increase in the deviatoric stress that could destabilize faults in the subsurface. These changes in pore pressure and stress levels provide valuable insights into the dynamic behaviour of the geological formation and are crucial considerations in understanding the reservoir response to alterations in reservoir water levels. We contend that the rapid loading of the reservoir weakens this fault because of the undrained stress and pore pressure changes (Figure 7).

In addition, the megascopic representation of core samples in the configuration of the physical evidence illustrates that rock can exhibit relatively high porosities and low permeability when their pores are not well-connected (Figure 5). Thus, mica-schist may present preferential lateral fluid migration at depth, following the foliation direction. The surface rock beneath the Irapé reservoir is highly metamorphosed and generally has good porosity and low permeability. Therefore, pore pressure diffusion is disregarded as the potential cause triggering the seismicity at Irapé.

https://doi.org/10.5194/egusphere-2024-166
Preprint. Discussion started: 27 February 2024

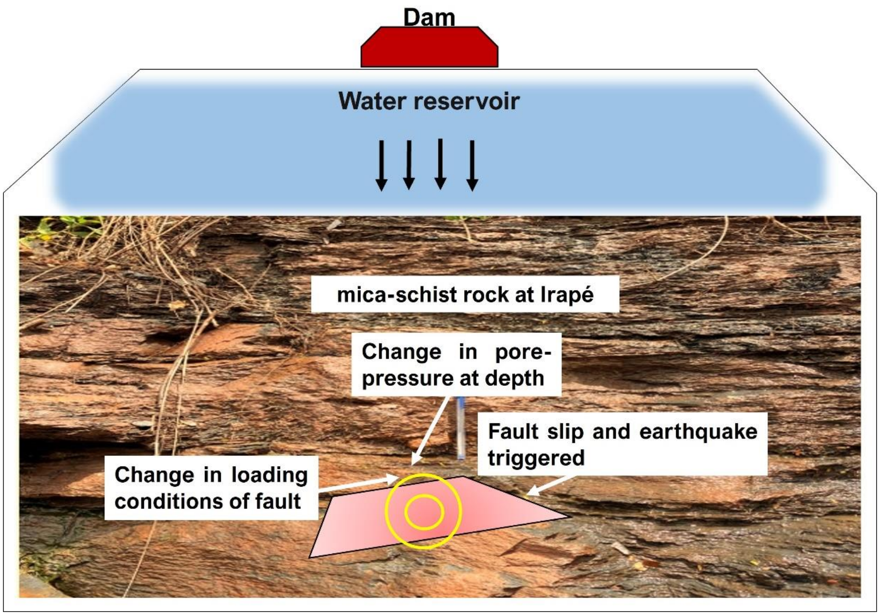

Figure 7. Schematic description of the mechanism of RTS at Irapé, indicating the effect of the weight of the reservoir water volume due to undrained response in low-permeable mica-schist rock (the background photo was taken in the field from an outcrop at Irapé).

The regional geology at the eastern part of the São Francisco Craton in the State of Minas Gerais follows a N-S direction (Almeida, 1977). Silva et al. (2014) also mentioned that the repetition of a structural trend in the NE-SW direction originates from the geological and geophysical structuring of the crust. This trend makes it feasible to assume the existence of a N-S vertical mature fault that could become destabilized by small changes in the effective stress. An association of such seismicity with the shear zone along reservoir /lineaments suggests the reactivation of such faults under the influence of reservoir impoundment.

To mitigate the risk of RTS, it is crucial to thoroughly characterize the site by measuring rock physical properties. Analytical and numerical solutions should integrate the physics of the problem, such as poromechanics to assess both the undrained response of the subsurface to reservoir impoundment and pore-pressure diffusion. Such models should include the rock layers below the reservoir down to the crystalline basement and their characteristics, including features like faults. Before the construction of

https://doi.org/10.5194/egusphere-2024-166
Preprint. Discussion started: 27 February 2024

the dam, the hazard of triggering moderate to large earthquakes should be estimated, to disregard locations with high probability of RTS. This estimation requires knowing the hydro-mechanical properties of the rock layers, i.e., permeability, porosity, stiffness, and strength, as well as the design parameters of the dam, i.e., height. The successful management of RTS requires an interdisciplinary approach combining concepts of hydrogeology, geomechanics and seismology.

Finally, to address and manage RTS risks, the traffic light protocol (TLP) is being employed. In general, TLP initiates the green light as the primary approach allowing operations without restrictions, the yellow light as the point to activate mitigation measures, and the red light as the point necessitating regulatory intervention. The efforts have also begun by linking the configuration of TLPs with risk-oriented measures, infrastructure harm, and the likelihood of loss or damages while adapting them to real-time data. The occurrences that may ensure after an operation are crucial, given their substantial impact on standard risk management. Nevertheless, these methodologies can be revolved around by assessment of events succeeding in the conclusion of an operation. The utilization of physics-based models holds promising by illustrating and projecting anticipated seismic activity, enabling the anticipation of future warnings and risks, and build up the information for operational adjustments and for future mitigation (Boyet et al., 2023b) (Figure 8).

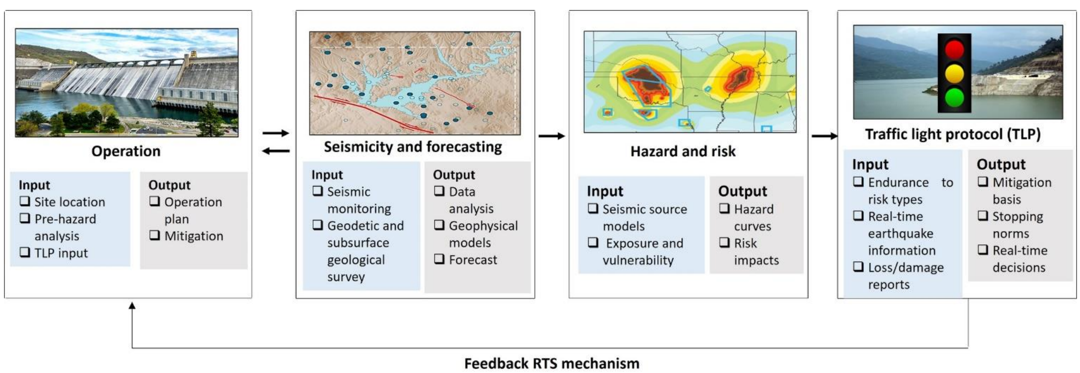

https://doi.org/10.5194/egusphere-2024-166
Preprint. Discussion started: 27 February 2024

Figure 8. Reservoir operations and impoundment are strategically designed to reduce the risk of RTS. Monitoring seismic and geophysical activities yields information for predictive earthquake models. The catalogues of earthquakes and source/origin models are applicable in the assessment of hazard and risk. These assessments of risk and hazard can guide the development of a traffic light protocol (TLP), functioning as a dynamic decision module during operations. The display of each box shows the classifications of input data (blue boxes) and output results (grey boxes).

Regarding the mitigation approaches for RTS within the framework of a TLP, the effectiveness of an operator heavily relies on the efficiency of mitigation strategies implemented at the yellow-light stage. Ideally, these strategies would proficiently diminish seismic risks and hazards, ultimately circumventing the red-light scenario that terminates the operation. Thus, TLPs can be one major strategy and strong decision-making tool for operators to minimize the risk of RTS for future developments of dams.

6.Conclusions

We have analysed RTS at Irapé to discern the cause of the triggered seismicity. The measured low permeability of the rock at Irapé disregards pore pressure diffusion as the triggering mechanism and suggests that the M3.0 RTS was triggered by the undrained response of the subsurface to reservoir impoundment. Analytical calculations estimate that pore pressure increased by 0.54 MPa in response to an increase of 136 m in the reservoir-water level. The resulting vertical effective stress increased by 0.82 MPa and the horizontal effective stress decreased by 0.34 MPa. Thus, the deviatoric stress would increase in a normal faulting stress regime, like the one at Irapé, destabilizing the fault and causing RTS. Both laboratory measurements and analytical calculations support the hypothesis that the initial seismicity was triggered by the undrained response of the subsurface to the loading of the reservoir at Irapé. This study also suggests that the occurrence of such earthquakes may be avoided by carefully manipulating reservoir loading.

Data availability

The data analysed and /or used in this study are presented in the Supplementary Material.

https://doi.org/10.5194/egusphere-2024-166
Preprint. Discussion started: 27 February 2024

Supplementary Material

The Supplementary Material related to this article is available online.

Author contributions

H.R., G.S.F., V.V. co-designed the study. E.S. and H.R. did sampling. H.R. wrote the paper performed laboratory measurements. H.R. and V.V. did the analytical calculations. G.S.F. and V.V. reviewed, contributed to the interpretation of the results, and edited the paper.

Competing interests

The corresponding and co-authors state that there are no competing interests.

Acknowledgments

This study was financed in part by the Coordenação de Aperfeiçoamento de Pessoal de Nível Superior -Brasil (CAPES) -Finance Code 001. The authors acknowledge funding from the Spanish National Research Council (CSIC) under the Program for Scientific Cooperation iCOOP+ through the Project COOPA20414. V.V. acknowledges funding from the European Research Council (ERC) under the European Union's Horizon 2020 Research and Innovation Program through the Starting Grant GEoREST(www.georest.eu) under Grant agreement No. 801809. IMEDEA is an accredited "Maria de Maeztu excellence Unit" (Grant CEX2021-001198, funded by MCIN/AEI/ 10.13039/501100011033). G.S.F gratefully acknowledges CNPq (Grant 310240/2020-4 PQ-1C). G.S.F. and H.R. and E.S. also thank to INCTET-CNPq (Institutos Nacionais de Ciência e Tecnología de estudos tectónicos) Brazil. We thank to Prof. Carlos Jorge de Abreu for conducting samples measurements at Laboratory of Physical Properties of Rocks at the University of Brasília.

References

Almeida FFM 1977. The São Francisco Craton. Brazilian Journal of Geosciences, 7:349-364.

API, 1998. Recommend Practices for Core Analysis. RP40. American Petroleum Institute. 2nd Edition.

https://doi.org/10.5194/egusphere-2024-166
Preprint. Discussion started: 27 February 2024

Araujo Filho, J. O; Silva, G. F; Lima, E. A. M; Ferreiara, V. N; Batista, O. C. A; Franca, G. S. 2010. Mapeamento Geoestrutural da área de influência da Usina Hidrelétrica de Irapé, Grão Mogol, MG. Anais do 45º Congresso Brasileiro de Geologia, Sociedade Brasileira de Geologia.

Arora, K., Srinu, Y., Gopinadh, D., Chadha, R.K., Raza, H., Mikhailov, V., Ponomarev, A., Kiseleva, E. and Smirnov, V. Lineaments in Deccan Basalts: The Basement Connection in the Koyna–Warna RTS Region. Bull. Seismol. Soc. Amer., v.108 (5), DOI: 10.1785/0120180011 (2018).

Assumpção, M; Feng, M; Tassara, A; Julia, J. 2012. Models of crustal thickness for South America from seismic refraction, receiver functions and surface wave tomography. Tectonophysics, 609:82-96.

Bell, M.L., Nur, A., 1978. Strength changes due to reservoir-induced pore pressure, stresses, and application to Lake Oro-Berrocal. J. Geophys. Res. 83, 4469–4483.

Boyet, A., De Simone, S., Ge, S. et al. Poroelastic stress relaxation, slip stress transfer and friction weakening controlled post-injection seismicity at the Basel Enhanced Geothermal System. Commun Earth Environ 4, 104 (2023). https://doi.org/10.1038/s43247-023-00764-y

Boyet, A., De Simone, S., Vilarrasa, V.; Physics-Based Modeling to Understand and to Propose Forecasting Methods of Induced Seismicity. Seismological Research Letters 2023; 94 (6): 2666–2678. doi: https://doi.org/10.1785/0220230109

Carder, D. S. (1945). Seismic investigation in the Boulder Dam area, 1940-1944, and the influence of reservoir loading on earthquake activity, Bull. Seism. Soc. Am. 35, 175-192.

Ceia Marco, Roseane Missagia, Ricardo Fasolo, Irineu Lima Neto, 2019. Relationship between porosity, permeability, and pore compressibility; DOI: 10.22564/16cisbgf2019.287

CEMIG - Minas Gerais Energy Company (2001). Geological observations in the UHE Irapé sector - Consultancy Report. Belo Horizonte, MG, 6p

Cesca, S., Braun, T., Maccaferri, F., Passarelli, L., Rivalta, E., and Dahm, T. (2013a). Source modelling of the M5–6 Emilia-Romagna, Italy, earthquakes (2012 May 20–29). Geophys. J. Int. 193, 1658–1672. doi: 10.1093/gji/ggt069

https://doi.org/10.5194/egusphere-2024-166
Preprint. Discussion started: 27 February 2024

Cesca, S., Grigoli, F., Heimann, S., González, Á, Buforn, E., Maghsoudi, S., et al. (2014). The 2013 September–October seismic sequence offshore Spain: a case of seismicity triggered by gas injection? Geophys. J. Int. 198, 941–953. doi: 10.1093/gji/ggu172

Chang, K.W., Yoon, H. Permeability-controlled migration of induced seismicity to deeper depths near Venus in North Texas. Sci Rep 12, 1382 (2022). https://doi.org/10.1038/s41598-022-05242-7

Chen, L., & Talwani, P. (2001). Mechanism of initial seismicity following impoundment of the Monticello Reservoir, South Carolina. Bulletin of the Seismological Society of America, 91(6), 1582-1594.

Chimpliganond, C., G. S. França, A. E. Bandeira, and L. Bevilaqua (2007). Reservoir-triggered seismicity at the highest Brazilian dam, AGU 2007 —Meeting of Americas Joint Assembly Abstract, Acapulco, Mexico, Acapulco, Mexico, 22–25 May.

Cocco, M., Rice, J.M., 2002. Pore pressure and poroelasticity effects in Coulomb stress analysis of earthquake interactions. Journal of Geophysical Research 107. doi:10.1029/2000JB000138

Cornet, F. H., and J. Yin (1995), Analysis of induced seismicity for stress field determination and pore pressure mapping, Pure Appl. Geophysics., 145, 677–700

CPRM - Mineral Resources Research Company (2004). Project Registration of Groundwater Supply Sources. Jequitinhonha Valley: Diagnosis of the Municipality of Berilo-MG. Belo Horizonte, 43p

Crane, L. J., & Friedman, A. (1956). The diffusion of chemically reacting systems in a laminar flow of fluid. AIChE Journal, 2(2), 186-191

Developments in Structural Geology and Tectonics, Elsevier, Volume 5, 2019, Pages 119-128,

Ellsworth, W. L. (2013). Injection-induced earthquakes. Science 341, 1225942. doi: 10.1126/science.1225942

Foulger, G. R., Wilson, M., Gluyas, J., Julian, B. R., and Davies, R.: Global review of human-induced earthquakes, Earth-Sci. Rev., 178, 438–514, 2018.

França, G. S., Assumpção, M., Ribotta, L. C., Von Huelsen, M. G., and Chimpliganond, E. C. N., Updated compilation of reservoir triggered seismicity in Brazil, in 2010 The Meeting of the Americas (AGU – American Geophysical Union), Foz do Iguaçu, Paraná, Brazil, 2010.

https://doi.org/10.5194/egusphere-2024-166
Preprint. Discussion started: 27 February 2024

Golstein, P; Snoke, A. 2005. "Sac Availability for the Iris Community" Incorporated Institutions for Seismology Data Management Center Eletronic Newsletter. Disponível em: Acessado em: 15 de dezembro de 2013

González, P. J., Tiampo, K. F., Palano, M., Cannavó, F., and Fernández, J. (2012). The 2011 Lorca earthquake slip distribution controlled by groundwater crustal unloading. Nat. Geosci. 5, 821–825. doi: 10.1038/ngeo1610

Gough, D.I., Gough, W.I., 1970a. Stress and deflection in the lithosphere near Lake Kariba, 1. Geophys. J. Int. 21, 65–78.

Golstein P. & Snoke A. 2005. "Sac Avaliability for the Iris Community" Incorporated Institutions for Seismology Data Management Center Eletronic Newsletter. Disponível em: <http://www.iris.edu/news/newsletter/vol7no1/page1.htm>. Acesso em: 15 dez 2013. » http://www.iris.edu/news/newsletter/vol7no1/page1.htm

Gough, D.I., Gough, W.I., 1970b. Load-induced earthquakes at Kariba, 2. Geophys. J. Int. 21, 79–101.

Grigoli, F., Cesca, S., Rinaldi, A. P., Manconi, A., López-Comino, J. A., Clinton, J. F., et al. (2018). The November 2017 Mw 5.5 Pohang earthquake: a possible case of induced seismicity in South Korea. Science 360, 1003–1006. doi: 10.1126/ science.aat 2010

Gupta, H. K., K. Arora, N. P. Rao, S. Roy, V. M. Tiwari, P. et al., Investigations of continued reservoir triggered seismicity at Koyna, India, Geol. Soc. Lond. Spec. Publ. 445, 151–188 (2016).

Gupta, H. K.: A review of recent studies of triggered earthquakes by artificial water reservoirs with special emphasis on earthquakes in Koyna, India, Earth-Sci. Rev. 58, 279–310, https://doi.org/10.1016/S0012-8252(02)00063-6, 2002.

Keranen, K. M., Savage, H. M., Abers, G. A., and Cochran, E. S. (2013). Potentially induced earthquakes in Oklahoma, USA: Links between wastewater injection and the 2011 Mw 5.7 earthquake sequence. Geology 41, 699–702. doi: 10.1130/ G34045.1

Keranen, K. M., Weingarten, M., Abers, G. A., Bekins, B. A., and Ge, S. (2014). Sharp increase in central Oklahoma seismicity since 2008 induced by massive wastewater injection. Science 345, 448–451. doi: 10.1126/science.125 5802

https://doi.org/10.5194/egusphere-2024-166
Preprint. Discussion started: 27 February 2024

Kim, K.-H., Ree, J.-H., Kim, Y., Kim, S., Kang, S. Y., and Seo, W. (2018). Assessing whether the 2017 Mw 5.4 Pohang earthquake in South Korea was an induced event. Science 360, 1007–1009. doi: 10.1126/science. aat6081

Kivi, I. R., Boyet, A., Wu, H., Walter, L., Hanson-Hedgecock, S., Parisio, F., and Vilarrasa, V.: Global physics-based database of injection-induced seismicity, Earth Syst. Sci. Data, 15, 3163–3182, https://doi.org/10.5194/essd-15-3163-2023, 2023.

Lee, W. H. K; Lahr, J. C, 1975. HYPO 1971 (revised a computer program for determining hypocentre, magnitude and first motion pattern of local earthquakes. USGS, Open file report. 64 p.

Lima SAA, Martins-Neto MA, Predrosa-Soares AC, Cordani UG, Nutman A. 2002. The Salinas Formation in the Type Area, NE of Minas Gerais: a proposal to review the stratigraphy of the Araçuaí Belt based on sedimentary and metamorphic evidence and U-Pb SHRIMP ages. Brazilian Journal of Geosciences, 34(4):491-500.

Marshak, S; Alkmim, F. F.; Whittington; Pedrosa-Soares, A. C. 2006. Extensional collapse in the Neoproterozoic Araçuaí orogen, eastern Brazil: a setting for reactivation of asymmetric crenulation cleavage. Journal of Structural Geology, 28(1):129-147.

McGarr, A., Simpson, D., and Seeber, L. (2002). 40—Case histories of induced and triggered seismicity. Int. Geophys. 81A, 647–661.

Neuzil, C. E. (1986). Groundwater flow in low-permeability environments. Water Resources Research, 22(8), 1163-1195.

PLANVALE-Water Resources Master Plan for the Jequitinhonha and Pardo Valleys (1994). Diagnostic Report carried out by Geotécnica and DHV Consultants BV, Annex B, Hydrogeology, 133p.

Raza, H., Kivi, I.R., França, G.S. and Vilarrasa V. Reservoir impoundment-triggered seismicity in Brazil: the case of M4.0 Nova Ponte earthquake. Sci Rep 13, 22226 (2023). https://doi.org/10.1038/s41598-023-48924-6

Rice, J.R. and Cleary, M.P. (1976) Some basic stress-diffusion solutions for fluid-saturated elastic porous media with compressible constituents. Rev. Geophys. Space Phys., v.14, pp.227-241.

https://doi.org/10.5194/egusphere-2024-166
Preprint. Discussion started: 27 February 2024

Roeloffs, E.A., 1988. Fault stability changes induced beneath a reservoir with cyclic variations in water level. J. Geophys. Res. 93, 2107–212

Rutqvist, J. (2012). The geomechanics of CO_2 storage in deep sedimentary formations. Geotechnical and Geological Engineering, 30, 525-551.

Sausse, J., Fourar, M. and Genter, A. (2006) Permeability and alteration within the Soultz granite inferred from geophysical and flow log analysis. Geothermics, v.35(5-6), pp.544-560.

Sayão, E., França, G. S., Holanda, M., and Gonçalves, A.: Spatial database and website for reservoir-triggered seismicity in Brazil, Nat. Hazards Earth Syst. Sci., 20, 2001–2019, https://doi.org/10.5194/nhess-20-2001-2020, 2020

Silva, G. F., J. O. Araújo Filho, M. G. Von Huelsen, C. N. Chimpliganond, and G. S. França (2014). Influence of Brazilian structures on the reservoir-induced seismicity case of Irapé Hydroelectric Plant, Minas Gerais, Brazil, Braz. J. Geol. 44, no. 3, 375–386, DOI: 10.5327/Z2317-4889201400030004.

Simpson, D.W. (1976) Seismicity change associated with the reservoir loading. Engg. Geol., v.10, pp.123-150.

Simpson, D.W., Leith, W.S. and Scholz, C.H. (1988) Two types of reservoirs induced seismicity. Bull. Seism. Soc. Amer., v.78, pp.2025–2040.

Simpson, DW 1986. Triggered Earthquakes. Annual Review Earth Planetary Sciences, 14: 21-42.

Skempton, A. W. (1954). The pore-pressure coefficients A and B. Geotechnique, 4(4), 143-147.

Snow, D.T., 1972. Geodynamics of seismic reservoirs. Proceedings of the Symposium on Percolation through Fissured Rocks. Deutsche Gessellschaft für Erd- und Grundbau, Stuttgart, Germany, pp. 1–19 (T2-J).

Talwani, P. and Acree, S. (1984/85), Pore pressure diffusion and mechanism of reservoir induced seismicity. Pure and applied Geophysics 122,947-965

Todd, D. K., & Mays, L. W. (2005). Groundwater Hydrology

Vilarrasa, V., Carrera, J., Olivella, S., Rutqvist, J., and Laloui, L.: Induced seismicity in geologic carbon storage, Solid Earth, 10, 871–892, https://doi.org/10.5194/se-10-871-2019, 2019.

https://doi.org/10.5194/egusphere-2024-166
Preprint. Discussion started: 27 February 2024

Vilarrasa, V., De Simone, S., Carrera, J. et al. Multiple induced seismicity mechanisms at Castor underground gas storage illustrate the need for thorough monitoring. Nat. Commun. 13, 3447 (2022). https://doi.org/10.1038/s41467-022-30903-6

Vilarrasa, V., De Simone, S., Carrera, J., and Villaseñor, A.: Unravelling the causes of the seismicity induced by underground gas storage at Castor, Spain, Geophys. Res. Lett., 48, e2020GL092038, https://doi.org/10.1029/2020GL092038, 2021

Vilarrasa, V., Makhnenko, R. & Gheibi, S. 2016. Geomechanical analysis of the influence of CO_2 injection location on fault stability. Journal of Rock Mechanics and Geotechnical Engineering. 8(6):805–818.

Vilarrasa, V., Raza, H., Kivi, I. R., and França, G. S.: Understanding the triggering mechanisms of reservoir-triggered seismicity at Nova Ponte, Brazil, through hydro-mechanical modeling, EGU General Assembly 2023, Vienna, Austria, 24–28 Apr 2023, EGU23-11711, https://doi.org/10.5194/egusphere-egu23-11711, 2023.

Wever, T. H. 1989. The Conrad discontinuity and the lop of the reflective lower crust – do they coincide? Tectonophysics,157:39-58.

Yeck, W. L., Weingarten, M., Benz, H. M., McNamara, D. E., Bergman, E. A., Herrmann, R. B., et al. (2016). Far-field pressurization likely caused one of the largest injections induced earthquakes by reactivating a large preexisting basement fault structure. Geophys. Res. Lett. 43, 10198–10207. doi: 10.1002/2016GL07 0861.